Journal of Nuclear Medicine, published on September 17, 2015 as doi:10.2967/jnumed.115.156067

Metabolic topology of neurodegenerative disorders – influence of cognitive and motor deficits

Running title: Metabolic topology

Oliver Granert[1*], Alexander E. Drzezga[2], Henning Boecker[3], Robert Perneczky[4,5,6], Alexander Kurz[6], Julia Götz[1], Thilo van Eimeren[1], Peter Häussermann[7,8*]

[1]Department of Neurology, Kiel University, Germany

[2]Department of Nuclear Medicine, University of Cologne, Germany

[3]Department of Radiology, Bonn University, Germany

[4]Neuroepidemiology and Ageing Research Unit, Imperial College of Science, Technology and Medicine, London, United Kingdom

[5]Cognitive Impairment and Dementia Services, West London Mental Health NHS Trust, United Kingdom

[6]Department of Psychiatry, TU Munich, Germany

[7]Department of Psychiatry, Kiel University, Germany

[8]LVR Clinic Cologne, Academic teaching hospital, University of Cologne, Germany

*Corresponding author

Oliver Granert, Dipl. Inf.

Department of Neurology, Kiel University

Arnold-Heller-Str. 3

24105 Kiel

Germany

E-Mail: *o.granert@neurologie.uni-kiel.de*

phone: +49 431 597 8823

Total word count: 5094

ABSTRACT

Parkinson's disease with and without dementia (PDD and PD), dementia with Lewy-bodies (DLB), and Alzheimer dementia (AD) traditionally have been viewed as distinct clinical and pathological entities. However, intriguing overlaps in biochemical, clinical, and imaging findings question the concept of distinct entities and suggest a continuous spectrum in which individual patients express PD-typical patterns and AD-typical patterns to a variable degree.

Methods: Following this concept, we built a topological map based on regional patterns of the cerebral metabolic rate of glucose (rCMRglc) as measured with ^{18}F-fluorodeoxyglucose-PET (^{18}F-FDG-PET) to rank and localize single subjects' disease status according to PD-typical (PD vs. controls) and AD-typical (AD vs. controls) pattern expression in patients clinically characterized as PD, PDD, DLB, amnestic mild cognitive impairment (aMCI) and AD.

Results: The topology generally confirmed an indivisible spectrum of disease manifestation according to two separable expression patterns (PC_{cog}, PC_{mot}). PC_{cog} expression values were highly correlated with individual cognitive, but not motor disability, whereas the opposite was found for PC_{mot}.

Conclusion: The metabolic imaging analysis support the notion that there is a continuous spectrum of neurodegeneration between AD and PD. Furthermore, PDD and DLB may in fact represent one overlapping disease entity, characterized by the presence of mixed neuropathology and only different by the time course.

Keywords: Alzheimer, Parkinson, FDG PET, dementia, motor deficits

INTRODUCTION

Age-related neuropsychiatric disorders such as Parkinson's disease with and without dementia (PDD and PD), dementia with Lewy-bodies (DLB), amnestic mild cognitive impairment (aMCI), and Alzheimer disease dementia (AD) represent a growing socioeconomic challenge. However, these disorders show substantial clinical and neuropathological overlap, limiting diagnostic accuracy, and questioning the concept of distinct clinical entities *(1–3).* Indeed, the notion that PD and AD may be extremes of a spectrum of neurodegenerative diseases – with DLB and PDD presenting overlapping neuropathological and clinical features within this spectrum – has received growing attention in recent years *(4).*

While pathophysiologically and clinically different, PD and AD share some aspects in common: Both are age-related neurodegenerative disorders characterized by aggregation of pathological proteins leading to dysfunction of cerebral networks and distinct patterns of metabolic changes *(3–6).* Cases characterized by “pure” PD (α-synuclein aggregation) or “pure” AD (amyloid- and tau aggregation) pathology do not represent the majority of affected patients. Biologically and histopathologically, there is an overlap of these age-associated proteinopathies. They form a continuum with concomitant amyloid-, tau- and α-synuclein aggregation as well as microvascular changes *(6,7).*

Amnestic MCI (aMCI) represents an intermediate clinical state of cognitive decline between normal aging and AD, showing histopathological and neurobiochemical similarities to AD *(8,9).* DLB and PDD are also age-related neurodegenerative disorders sharing clinical and histopathological aspects with both, PD and AD *(7,10).* Hence, they can be seen as intermediate neurodegenerative disorders in a spectrum between “pure”

Parkinson`s and “pure” Alzheimer`s disease. As the pattern of histopathology, neuronal network dysfunction and associated clinical deficits is indeed continuous, the traditional view of distinct disease entities is increasingly being questioned.

A biomarker-based approach targeted to disentangle histopathology-clinical relationships within this spectrum may further help to guide classification of neurodegenerative disorders and treatment stratification. ^{18}F-fluorodesoxyglucose (FDG) is an established imaging biomarker of neurodegeneration. In AD, characteristic deficits of rCMRglc involve temporo-parietal and posterior cingulate cortices *(11).* FDG uptake in PD is most consistently characterized by metabolic changes within fronto-temporal and parieto-occipital areas *(12–14).*

In this study, we aimed to explore the spectrum of the most common age-related neurodegenerative disorders, ranging from Parkinson`s to Alzheimer`s disease on a metabolic level. In contrast to previous studies on this topic, using pair-wise group comparisons of different disease groups, we were especially interested in the analysis of different disease groups in relation to the parkinsonian and dementia-related marginal patterns (AD and PD vs controls). Our goal was to metabolically explore the full neurodegenerative spectrum (PD-PDD-DLB-aMCI-AD) and depict it in one common topological map.

METHODS

Participants

The analysis was based on a cohort of 100 patients with aMCI, 91 patients with AD, 20 patients with PD, 17 patients with PDD, 26 patients with DLB as compared to 24 elderly controls (CON). All subjects underwent whole brain ^{18}F-FDG-PET under resting conditions. Structural imaging (CT or MR) was performed in all participants to exclude structural abnormalities of the brain beyond cortical atrophy.

Patients with aMCI/AD were recruited from a university memory clinic, while patients with PD, PDD and DLB were recruited from a university movement disorder clinic. Patients with AD met NINCDS/ADRDA criteria for probable AD *(15).* None of the patients with AD or aMCI showed parkinsonian symptoms. All patients were seen both by a movement disorder specialist and a psychiatrist from the memory clinic. Diagnosis of PD was made by consensus between experienced clinicians using the UK brain bank criteria for PD *(16).* The severity of parkinsonian motor symptoms was rated using the UPDRS III motor scale *(17).* Dementia in PD was diagnosed according to the Diagnostic and Statistical Manual of Mental Disorders (DSM-IV) and consensus criteria for PDD *(10,18).* DLB was diagnosed according to McKeith *(18),* whereas aMCI was diagnosed according to the International Working Group on MCI criteria *(19).* Neuropsychological evaluation was based on the battery of the Consortium to Establish a Registry for Alzheimer's disease (CERAD-NAB) scores *(20).*

Differences in the clinical and neuropsychological findings were assessed between groups using the non-parametric Mann-Whitney U test or chi-square test. Results are

given as mean values and corresponding standard deviations. P-values are two-tailed, and significance level was set at $p<0.05$.

In accordance with the Declaration of Helsinki, the experimental procedures were explained and written informed consent was signed by all subjects and, where appropriate, by their caregivers. The study had the approval of the local ethics committee and radiation protection authorities.

Positron Emission Tomography

Each patient fasted for at least 6 hours prior to PET scanning. Dopaminergic and cholinergic medication was transiently stopped at least 12 hours prior scanning. PET images were acquired in 3D mode using a Siemens ECAT EXACT HR+ scanner (CTI, Knoxville, TN., USA). Intravenous injection of 185 Mbq ^{18}F-FDG was performed with subjects being at rest (eyes closed, dimmed ambient light, no movement). A 20 minutes static acquisition protocol beginning thirty minutes post-injection was used. Transmission scans were obtained for attenuation correction purposes using a rotating ^{68}Ge/^{68}Ga-source. After corrections for randoms, dead time and scatter, images were reconstructed with filtered back-projection (Hamm filter, cut-off frequency 0.5 cycles/projection element) resulting in 60-63 slices in a 128×128 matrix (pixel size 2 mm) and inter-plane separation of 2.4 mm.

Pre-processing and Analysis of the Imaging Data

The PET image data were pre-processed and analysed with the SPM8 software (*Wellcome Department of Cognitive Neurology, London, UK*) and MATLAB 7.11.0.584

(*Mathworks Inc)*. Stereotactic normalization was performed using the SPM8 default PET template. The normalization resulted in a standardized image set in the Montreal Neurological Institute (MNI) space. The normalized images were smoothed with an isotropic Gaussian filter (12mm FWHM). Radioactivity distribution was analysed semi-quantitatively by normalizing regional cerebral ^{18}F-FDG-PET utilization by linear proportional scaling to a default value of 50 ml/dl/min.

For statistical analysis the pre-processed data sets were compared voxel-by-voxel between the marginal subgroups (AD and PD) of patients and the control group (CON) using two-sample t-tests, assuming unequal variances between the groups. To evaluate the spatial distribution of the metabolic differences between our marginal groups (AD, PD, CON) we calculated statistical t-maps for all possible group comparisons. For visualization purposes in Figure 1 and Supplemental Figure 1, the statistical threshold was set to $P_{unc}<0.001$ for all contrasts of interest (AD vs. CON, PD vs. CON and AD vs. PD) to show the full extent of metabolic differences.

All group-wise comparisons were visually inspected and compared to previous findings. However, detailed results of the statistical analyses are not reported here. We refer all interested readers to Teune et al. *(14)* where equivalent groups were systematically tested against a control group using a very similar image processing procedure with comparable results.

Pattern Analysis

Disease specific expression values of voxel-based spatial covariance patterns were determined using the t-map projection method *(21).* This approach is closely related to a

method described by Worsley et al. *(22),* assessing the global significance of pattern differences.

Mathematically, the projection method corresponds to the scalar product of two vectors, where the vectors are the concatenated intensity values of the voxels in the normalized and smoothed PET images (first vector) and the SPM t-maps (second vector). The resulting scalar (individual expression value) is used as one coefficient for the expression vector. To remove voxels with less discriminative power, we additionally applied a threshold of |T|>=2 to the statistical maps. Using the t-maps of the contrasts AD-CON and PD-CON to project subject specific metabolic patterns gave two dimensional expression vectors representing the manifestation of the disease specific rCMRglc pattern for each subject. The first dimension represents the “Alzheimer-like” metabolic pattern, whereas the second corresponds to the “Parkinson-like” metabolic pattern. Decorrelation of the two expression scores was realized by a principal component based whitening transformation. The resulting new whitened feature space represents our “metabolic topological map”. To access the informative value of these new features, we analysed the feature space in three different ways:

First, we estimated these new features for all our subjects in all groups (AD, PD, PDD, DLB, aMCI and CON). The corresponding features were plotted into the two-dimensional topographic feature space (Fig. 2A-C) for visual presentation of the feature distribution. Secondly, we evaluated the two dimensions of our new remapped (decorrelated) feature vectors for correlations with the most important clinical features in our setting (cognitive deficits, i.e. MMSE-scores and extrapyramidal motor disturbances, i.e. UPDRS III-scores). The correlations were tested with non-parametric Spearman correlation tests (Fig. 3).

Finally, a group-wise analysis was performed by a Kruskal-Wallis chi-squared test followed by Wilcoxon post-hoc-tests to access statistical relevant differences of the topological features between groups. All statistical tests were performed using an alpha-level of $p<0.05$.

RESULTS

Clinical Data

Demographic and clinical variables are displayed in Table 1 and 2. All groups have similar age-ranges (mean age in groups 68-71) except for the group of aMCI-patients, which was slightly younger (mean age 65). The MMSE scores can be divided into three partitions. The first partition is the non-demented partition (CON, PD), the second partition is represented by the groups with a strong cognitive impairment (AD, DLB, PDD) whereas the third partition with the aMCI group lies between the two other partitions and shows significantly different MMSE-values as compared to the other groups. The UPDRS III scores were only available for the groups with motor deficits (DLB, PD and PDD). The motor deficits were comparable in the DLB and PD group, while the patients with PDD had significantly higher UPDRS III scores as compared to patients with PD and DLB.

Metabolic Pattern Comparisons between Marginal Groups

The voxel-wise SPM group comparisons with the control (CON) group and the two marginal groups (PD and AD) exhibited typical and distinct metabolic profiles for both the PD as well as the AD group (Fig. 1). The Alzheimer group (AD vs CON) showed a decline of rCMRglc bilaterally in the posterior cingulate cortex, the lateral temporal lobe (BA 20/21) and the inferior parietal cortex. Temporo-parietal and posterior cingulate reductions of rCMRglc in the group of AD patients is in accordance with previous imaging studies *(14,23–26)* (Fig. 1A). The group of patients with PD (PD vs CON) exhibited frontal and parieto-occipital hypometabolism as well as temporal and ponto-cerebellar hypermetabolism (Fig. 1B, 4B). This pattern is very closely related to a previous neuroimaging study using proportionally scaled datasets *(14).*

Finally, we compared the groups DLB and PDD using two sample t-tests and found no metabolic differences between these groups neither on peak nor on cluster level ($P_{FWE}<0.05$).

Calculation and Evaluation of Topological Features

Projection of the individual rCMRglc maps onto these disease specific patterns provided two expression values for the subjects of all groups showing a high correlation (Fig. 2A). Transformation by a decorrelation mapping (whitening transform) to a principal component (PC) aligned coordinate frame revealed the meaningful patterns in the feature space (Fig. 2B and 2C). The first PC (labelled PC_{cog} according to the correlation with MMSE) captures most of the variance of the original projection data, whereas the

second PC (labelled PC_{mot} according to the correlation with UPDRS III) captures the orthogonal variance.

To validate the expression values, we tested for correlations with clinical scores. The first dimension (PC_{cog}) of the features vectors showed high correlation with the MMSE score (rho=-0.617**;** P<<0.001) and no relation to the motor related UPDRS III score (rho=0.013; P=0.828), whereas the second dimension (PC_{mot}) showed no correlation with the dementia score MMSE (rho=0.069; P=0.59) but strong correlation with the UPDRS III score (rho=0.466; P<<0.001). A summary of the results of the correlation analysis is presented in Figure 3.

A further support of the informative value gave the group-wise comparisons. Here the expression values showed a significant group effect (Kruskal-Wallis chi-squared: PC_{cog} leads to X^2=136.5, df=5, P<<0.001; PC_{mot} leads to X^2=72.5, df=5, P<<0.001) and the post-hoc tests revealed the domain specific differences of the two feature dimensions. The detailed results of the post-hoc tests with the two components are given in Table 2.

The decorrelated features correspond to a decoupling of dementia (PC_{cog}) and motor (PC_{mot}) related symptoms. However, the metabolic patterns of these decorrelated features is also of interest and can deviate from the patterns of the original group comparisons. Therefore, we reconstructed the spatial metabolic patterns based on the whitening transform determined in the feature space. This reconstruction corresponds to a weighted recombination of the original (AD vs. CON) and (PD vs. CON) patterns according to the whitening transform and is visualized in Figure 4.

DISCUSSION

We built a topological map based on rCMRglc patterns measured with ^{18}F-FDG-PET. The map re-sampled a topology corresponding to clinical categorization and therefore can be used to rank and localize patients within this metabolic map (Fig. 2B-C). The Parkinson-related pattern as well as the dementia-related pattern are determined by metabolic changes which are important predictors of the individual disease status as well as the extent of neurodegeneration (Fig. 4).

The construction of this topological map is solely based on the two contrast patterns derived from the AD < CON and PD < CON comparisons with no statistical correction for clinical scores or severity of symptoms. However, the topological features PC_{cog} and PC_{mot}, representing each patient's position on the metabolic map, were clearly influenced by the severity of cognitive and motor deficits as shown by our correlation analysis (Fig. 3).

The SPM group comparisons showed the typical and well described metabolic characteristics *(Fig. 1, Supplemental Fig. 1*) of each group *(14).* Only PDD and DLB showed no significant differences in the SPM metabolic group comparison. These two groups have PC_{cog} and PC_{mot} features with a very strong overlap. Interestingly, clinical scores (MMSE and UPDRS III) in patients with PDD and DLB were also very similar. Taken together, the overlap in clinical scores, metabolic group comparisons as well as similarities in both measures of our principal component analysis further questions the artificial separation of PDD and DLB. DLB and PDD most probably represent overlapping neurodegenerative disorders with a very similar pathophysiology and pattern of metabolic changes, rather than distinctly different syndromes.

To validate and analyse our results in some more detail we start our discussion by looking at the two rCMRglc reference patterns. Our Alzheimer-pattern showed the well-described hypometabolism within the posterior cingulate cortex and in temporo-parietal cortical areas *(14,23–26).* Our Parkinson-pattern showed frontal and parieto-occipital hypometabolism (Fig. 1B, 4B) in accord with Teune et al. (14). In the literature, neuroimaging data in PD are heterogeneous, both concerning methodology and results *(28)*. Increases *(12)* as well as decreases *(27,28)* of glucose uptake within the basal ganglia have been reported in PD. Cortical metabolic abnormalities were reported in fronto-temporal and parieto-occipital areas *(12,14,29–32).*

The original expression values derived from these patterns from all subjects were correlated (Fig. 2A). This correlation implies that the expression values as well as their generating metabolic patterns cannot provide direct functionally specific information (because they were influenced by both diseases, PD and AD). The Figures 2B and 2C show the distribution of the decorrelated metabolic expression values and the position of each disease group in relation to the respective cognitive PC_{cog} and motor PC_{mot} metabolic pattern. Decoupling of the expression values into PC_{cog} and PC_{mot} expressions, achieved by the whitening transform, provides clearly functionally separated expressions and corresponding metabolic patterns (see correlation plots in Figure 3 and corresponding metabolic patterns in Figure 4).

The location of the mean expression vectors for each group (Fig. 2B) showed the centres of the CON, aMCI and AD group on a straight “pure dementia” line parallel to the PC_{cog} axis. Increased PD-like patterns in the PD, PDD and DLB groups were reflected in the topographic map by their location above this “pure dementia” line, showing higher PC_{mot} expression values. Of special interest were the mean locations of the PDD and

DLB groups. Both were located in direct neighbourhood to each other, reflecting the similarity of their metabolic representations. Post-hoc tests between these two groups showed no significant differences in PC_{cog} and PC_{mot} expression values. This finding in some sense contradicts the results presented in a discriminant analysis study *(33)* where the DLB and PDD groups were clearly distinguishable by their FDG-PET measurements. The reason for this discrepancy may be a result of the very low subject sample size (8 DLB patients and 4 PDD patients) in this previous study, which was discussed as major limitation of the study.

The group means of the PC_{cog} and PC_{mot} features of both the DLB as well as the PDD group are located above the AD group, corresponding to their motor deficits. This position of the PDD group in relation to the AD group is in accordance to a previous study *(34),* finding metabolic similarities between PDD and AD patients, but diverging rCMRglc reductions in the occipital cortex and visual association areas as represented in our motoric pattern PC_{mot} (Fig. 4B).

This also demonstrates that both, the AD and PD pattern, are represented in the metabolic measurements. These metabolic measurements are related to the severity of clinical symptoms as demonstrated by the correlation analysis (Table 2; Fig. 3). The existence of these strong correlations between metabolic and the clinical measurements qualifies the estimated features (PC_{cog} and PC_{mot}) as clinically meaningful. These features can be useful in supporting software tools to improve clinical differential diagnosis of age-associated neuropsychiatric disorders, i.e. memory decline and extrapyramidal motor disturbances.

The successful application of AD-related spatial patterns to PD and PDD patients has already been described *(35).* However, in our study, we used a voxel-based approach

without predefined regions of interest and additionally included the UPDRS III scores to detect extrapyramidal motor related patterns. We then applied a statistical method to disentangle the individual metabolic pattern into both a cognition and a motor related component showing similarities with previously reported motor and cognitive patterns in non-demented PD patients *(36)*. A detailed comparison is provided in the supplemental material (Section II and III; Suppl. Fig. 2a and 2b). However, both the clinical characteristics of our patient groups as well as the methods described here differ significantly from the studies summarized by Peng et al. *(36)*.

The representation of the measurements in the metabolic topographic map showed a considerable overlap between the features of the different disease groups. This overlap was most probably caused by similarities at the metabolic level in these groups. In some cases, clinically misclassified patients may also have contributed to this overlap. Nevertheless, we think that our data argue against a strict diagnostic categorisation of different neurodegenerative disorders. Rather, the calculated metabolic maps implicate that a continuum exists on the neuro-metabolic level in these ageing-associated disorders. Patients may benefit from a personalized treatment of motor and cognitive symptoms tailored for the individual patient instead of categorical treatment decisions. This may be difficult, as physicians are still trained to think in categories, and therapies were often designed for clearly defined categorical diagnosis. We think that a methodological approach as introduced in this study may provide objective information to guide personalized treatments and to possibly improve the health-related quality of life patients in the future.

Limitations of our study pertain to the lack of neuropathological confirmation of the clinical diagnosis. A proportion of patients might therefore be misclassified with respect

to a pathologically based classification *(35)*. However, our ranking methods did not rely on the unambiguous assignments and it was not the goal to provide such an assignment.

CONCLUSION

The metabolic measurements and derived motor (PC_{mot}) and cognitive (PC_{cog}) features add further neuroimaging support to the notion that there is a continuous spectrum of neurodegenerative disorders ranging from PD to AD. This metabolic topological map can furthermore aid to rank and localize elderly patients within the neurodegenerative spectrum. On an individual patient level, the map may help to facilitate clinical diagnosis and support pharmacological treatment decisions. Furthermore, our findings indicate that PDD and DLB may in fact represent one overlapping disease entity, characterized by the presence of mixed neuropathology and only different by the time course/onset of the individual sub-pathologies.

DISCLOSURE

No potential conflict of interest relevant to this article was reported.

REFERENCES

1. Ballard C, Ziabreva I, Perry R, et al. Differences in neuropathologic characteristics across the Lewy body dementia spectrum. *Neurology*. 2006;67:1931-1934.
2. Ince PG, Perry EK, Morris CM. Dementia with Lewy bodies. A distinct non-Alzheimer dementia syndrome? *Brain Pathol.* 1998;8:299-324.
3. Perl DP, Olanow CW, Calne D. Alzheimer's disease and Parkinson's disease: distinct entities or extremes of a spectrum of neurodegeneration? *Ann Neurol*. 1998;44:S19-S31.
4. Galpern WR, Lang AE. Interface between tauopathies and synucleinopathies: a tale of two proteins. *Ann Neurol*. 2006;59:449-458.
5. Perry EK, Irving D, Kerwin JM, et al. Cholinergic transmitter and neurotrophic activities in Lewy body dementia: similarity to Parkinson's and distinction from Alzheimer disease. *Alzheimer Dis Assoc Disord*. 1993;7:69-79.
6. Moussaud S, Jones DR, Moussaud-Lamodière EL, Delenclos M, Ross OA, McLean PJ. Alpha-synuclein and tau: teammates in neurodegeneration? *Mol Neurodegener*. 2014;9:43.
7. Irwin DJ, Lee VM-Y, Trojanowski JQ. Parkinson's disease dementia: convergence of α-synuclein, tau and amyloid-β pathologies. *Nat Rev Neurosci*. 2013;14:626-636.
8. Bertens D, Knol DL, Scheltens P, Visser PJ. Temporal evolution of biomarkers and cognitive markers in the asymptomatic, MCI, and dementia stage of Alzheimer's disease. *Alzheimers Dement*. 2015;11:511-522.

9. Lundström SL, Yang H, Lyutvinskiy Y, et al. Blood plasma IgG Fc glycans are significantly altered in Alzheimer's disease and progressive mild cognitive impairment. *J Alzheimers Dis*. 2014;38:567-579.
10. Emre M, Aarsland D, Brown R, et al. Clinical diagnostic criteria for dementia associated with Parkinson's disease. *Mov Disord.* 2007;22:1689-1707
11. Herholz K. FDG PET and differential diagnosis of dementia. *Alzheimer Dis Assoc Disord*. 1995;9:6-16.
12. Eidelberg D, Moeller JR, Dhawan V, et al. The metabolic topography of parkinsonism. *J Cereb Blood Flow Metab*. 1994;14:783-801.
13. Ma Y, Tang C, Spetsieris PG, Dhawan V, Eidelberg D. Abnormal metabolic network activity in Parkinson's disease: test-retest reproducibility. *J Cereb Blood Flow Metab*. 2007;27:597-605.
14. Teune LK, Bartels AL, de Jong BM, et al. Typical cerebral metabolic patterns in neurodegenerative brain diseases. *Mov Disord* 2010;25:2395-2404.
15. McKhann G, Drachman D, Folstein M, Katzman R, Price D, Stadlan EM. Clinical diagnosis of Alzheimer's disease: report of the NINCDS-ADRDA Work Group under the auspices of Department of Health and Human Services Task Force on Alzheimer's Disease. *Neurology*. 1984;34:939-944.
16. Hughes AJ, Daniel SE, Kilford L, Lees AJ. Accuracy of clinical diagnosis of idiopathic Parkinson's disease: a clinico-pathological study of 100 cases. *J Neurol Neurosurg Psychiatry*. 1992;55:181-184.
17. Fahn S. Assessment of the primary dystonias. In: Munsat T, ed. *The Quantification of Neurologic Deficit*. 1989:241-270.

18. McKeith IG. Consensus guidelines for the clinical and pathologic diagnosis of dementia with Lewy bodies (DLB): report of the Consortium on DLB International Workshop. *J Alzheimers Dis*. 2006;9:417-423.
19. Winblad B, Palmer K, Kivipelto M, et al. Mild cognitive impairment--beyond controversies, towards a consensus: report of the International Working Group on Mild Cognitive Impairment. *J Intern Med*. 2004;256:240-246.
20. Berres M, Monsch AU, Bernasconi F, Thalmann B, Stähelin HB. Normal ranges of neuropsychological tests for the diagnosis of Alzheimer's disease. *Stud Health Technol Inform*. 2000;77:195-199.
21. Soriano-Mas C, Pujol J, Alonso P, et al. Identifying patients with obsessive-compulsive disorder using whole-brain anatomy. *NeuroImage*. 2007;35:1028-1037.
22. Worsley KJ, Poline JB, Vandal AC, Friston KJ. Tests for distributed, nonfocal brain activations. *NeuroImage*. 1995;2:183-194.
23. Donnemiller E, Heilmann J, Wenning GK, et al. Brain perfusion scintigraphy with 99mTc-HMPAO or 99mTc-ECD and 123I-beta-CIT single-photon emission tomography in dementia of the Alzheimer-type and diffuse Lewy body disease. *Eur J Nucl Med*. 1997;24:320-325.
24. Herholz K, Salmon E, Perani D, et al. Discrimination between Alzheimer dementia and controls by automated analysis of multicenter FDG PET. *NeuroImage*. 2002;17:302-316.
25. Meltzer CC, Zubieta JK, Brandt J, Tune LE, Mayberg HS, Frost JJ. Regional hypometabolism in Alzheimer's disease as measured by positron emission tomography after correction for effects of partial volume averaging. *Neurology*. 1996;47:454-461.

26. Tam CWC, Burton EJ, McKeith IG, Burn DJ, O'Brien JT. Temporal lobe atrophy on MRI in Parkinson disease with dementia: a comparison with Alzheimer disease and dementia with Lewy bodies. *Neurology*. 2005;64:861-865.
27. Antonini A, Vontobel P, Psylla M, et al. Complementary positron emission tomographic studies of the striatal dopaminergic system in Parkinson's disease. *Arch Neurol*. 1995;52:1183-1190.
28. Berding G, Odin P, Brooks DJ, et al. Resting regional cerebral glucose metabolism in advanced Parkinson's disease studied in the off and on conditions with [(18)F]FDG-PET. *Mov Disord.* 2001;16:1014-1022.
29. Antonini A, De Notaris R, Benti R, De Gaspari D, Pezzoli G. Perfusion ECD/SPECT in the characterization of cognitive deficits in Parkinson's disease. *Neurol Sci.* 2001;22:45-46.
30. Firbank MJ, Colloby SJ, Burn DJ, McKeith IG, O'Brien JT. Regional cerebral blood flow in Parkinson's disease with and without dementia. *NeuroImage*. 2003;20:1309-1319.
31. Kuhl DE, Metter EJ, Riege WH, Markham CH. Patterns of cerebral glucose utilization in Parkinson's disease and Huntington's disease. *Ann Neurol*. 1984;15(suppl):119-125.
32. Piert M, Koeppe RA, Giordani B, Minoshima S, Kuhl DE. Determination of regional rate constants from dynamic FDG-PET studies in Parkinson's disease. *J Nucl Med.* 1996;37:1115-1122.
33. Garibotto V, Montandon ML, Viaud CT, et al. Regions of interest-based discriminant analysis of DaTSCAN SPECT and FDG-PET for the classification of dementia. *Clin*

Nucl Med. 2013;38:e112-e117.

34. Vander Borght T, Minoshima S, Giordani B, et al. Cerebral metabolic differences in Parkinson's and Alzheimer's diseases matched for dementia severity. *J Nucl Med.* 1997;38:797-802.
35. Weintraub D, Dietz N, Duda JE, et al. Alzheimer's disease pattern of brain atrophy predicts cognitive decline in Parkinson's disease. *Brain J Neurol*. 2012;135:170-180.
36. Peng S, Eidelberg D, Ma Y. Brain network markers of abnormal cerebral glucose metabolism and blood flow in Parkinson's disease. *Neurosci Bull*. 2014;30:823-837.

FIGURES

Fig 1: *Statistical maps used to calculate the expression values*

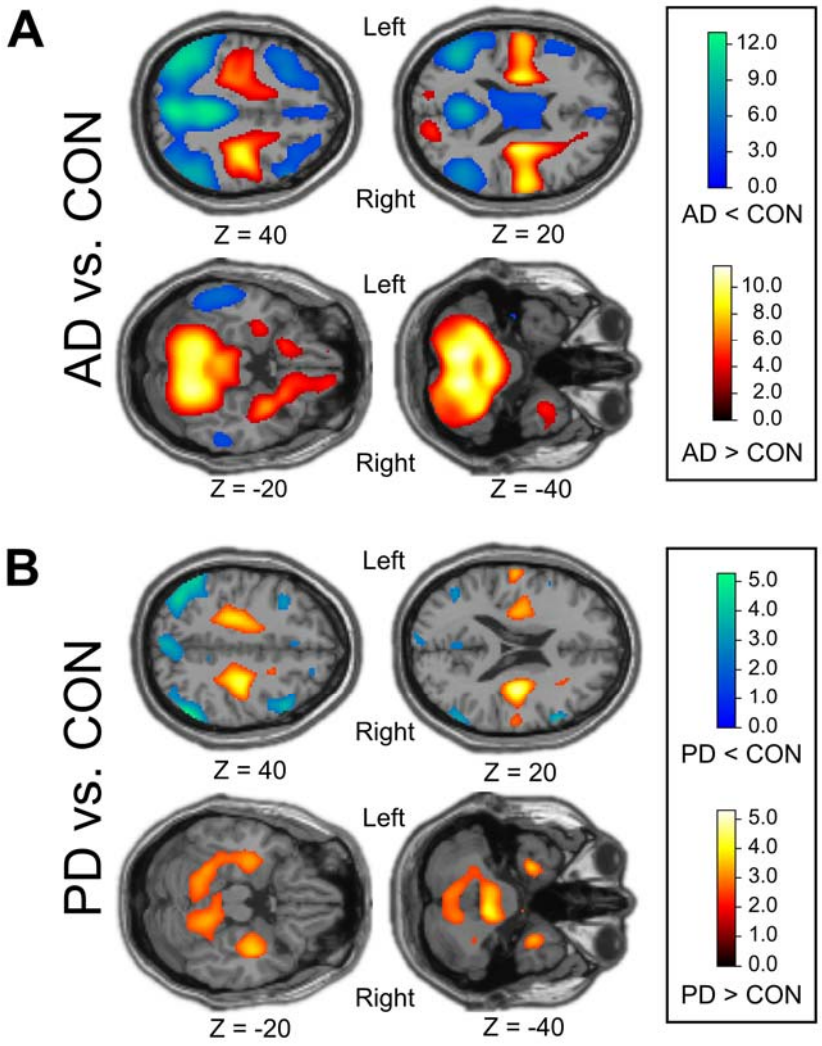

Panel A: *T-contrast AD versus CON* ***Panel B:*** *T-contrast PD versus CON. Statistical maps were shown with a threshold of* P_{unc}*<0.001 and overlaid onto the single subject T1 template.*

Fig 2: *The metabolic topological map*

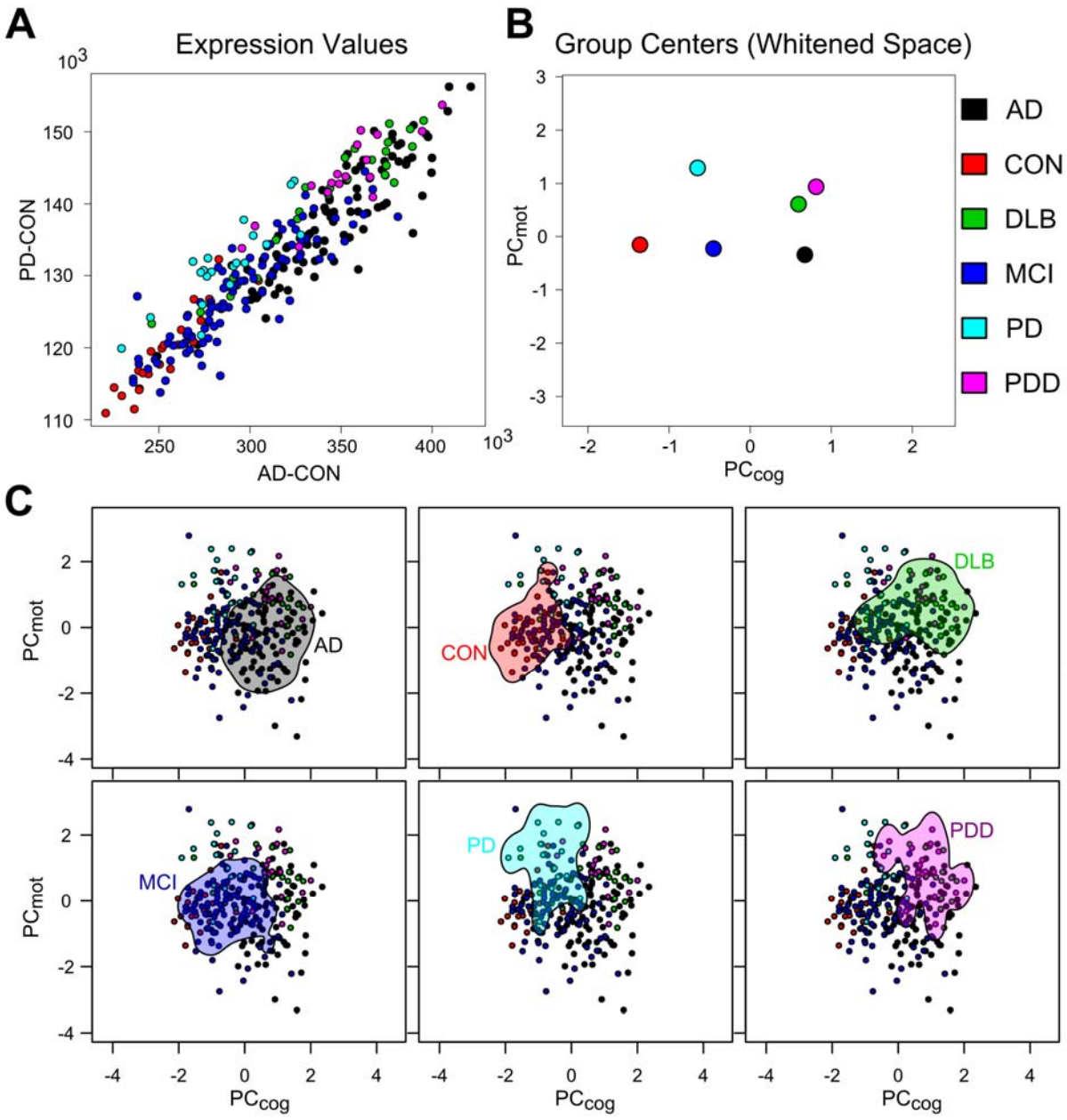

Panel *A:* *The statistical maps used to calculate the expression values correspond to the group t-contrasts: AD<CON and PD<CON.* **Panel *B:*** *Positions of the group means in normalized/whitened principal components space.* **Panel *C:*** *Distribution in the over-all normalized feature space (aligned and scaled along the two principal components* PC_{cog}

and PC_{mot}) with a coloured area inside the iso-curve of constant feature density for each of our patient groups.

Fig 3: Correlation between principal components and clinical scores

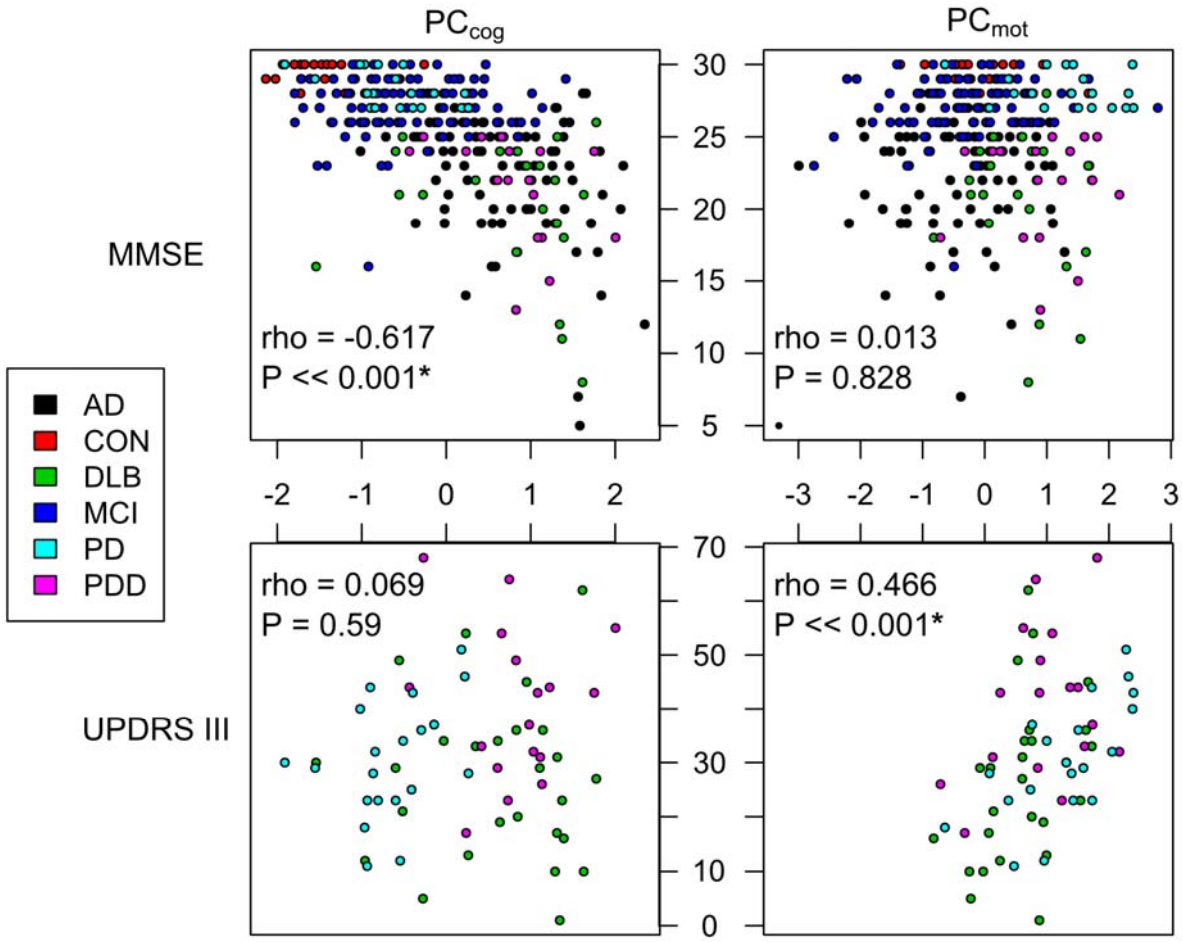

Projections to the principal components have a strong neg. correlation with the MMSE (PC_{cog}) and a strong positive correlation with the motor UPDRS III scale (PC_{mot}). The decomposition/whitening according to the principal component of the original datasets allows a differentiation of the clinical symptoms “cognitive deficits ” and “motor deficits“ based on their metabolic patterns.

Fig 4: Visualization of the principal patterns PC_{cog} and PC_{mot}

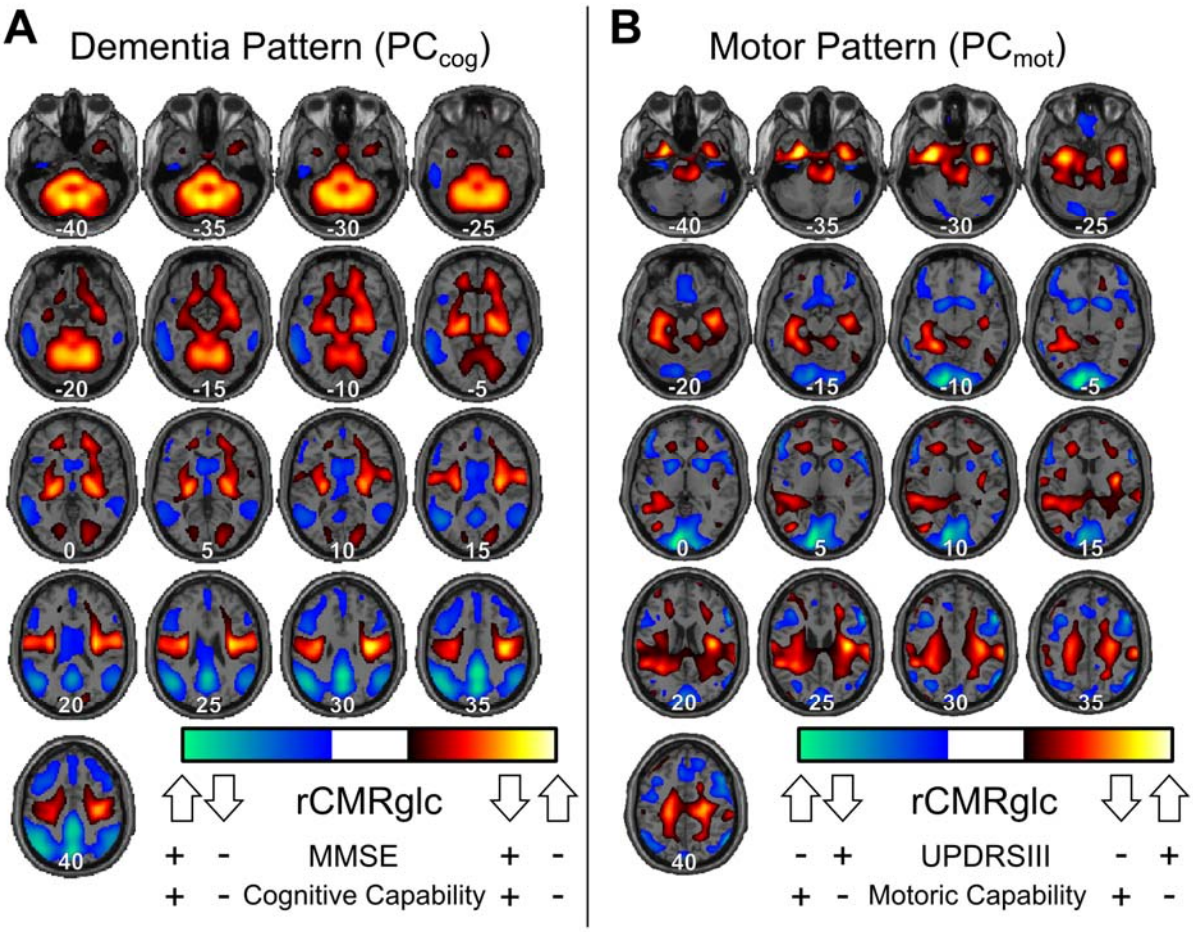

Panel A: Pattern related to PC_{cog} demonstrating high negative correlation with dementia score (MMSE). **Panel B:** Pattern related to PC_{mot} demonstrating high positive correlation with motor score (UPDRS III). Blue colours indicating regions with a positive correlation of cognitive and motor capabilities and rCMRglc, whereas red/yellow colours indicating regions were these capabilities are negatively coupled with rCMRglc measurements.

TABLES

Table 1: Group demographics

Group	N	Gender (m / f)	Age mean (sd)	MMSE mean (sd)	UPDRS III mean (sd)
AD	91	46 / 45	69.47 (7.78)	22.51 (4.25)	-
CON	24	12 / 12	69.92 (6.30)	29.38 (0.82)	0.3 (0.68)+
DLB	26	14 / 12	71.73 (6.50)	21.54 (5.34)	26.77 (15.01)
MCI	100	51 / 49	65.79 (9.06)	27.18 (2.00)	-
PD	20	14 / 6	67.65 (9.27)	28.25 (1.21)	30.65 (10.93)
PDD	17	14 / 3	70.76 (7.34)	21.41 (3.71)	40.71 (14.23)

(+ only N=10 UPDRS III measurements were available for the CON group)

Table 2: Metabolic and clinical group comparisons

	AD		**MCI**		**CON**		**DLB**		**PDD**		**PD**	
	MMSE	UPDRS III	MMSE	UPDRS III	MMSE	UPDRS III	MMSE	UPDRS III	MMSE	UPDRS III	MMSE	UPDRS III
AD			***	-	***	-	n.s.	-	n.s.	-	***	-
MCI	***	n.s.			***	-	***	-	***	-	*	-
CON	***	n.s.	***	n.s.			***	-	***	-	**	-
DLB	n.s.	***	***	***	***	***			n.s.	**	***	n.s.
PDD	n.s.	***	***	***	***	***	**n.s.**	**n.s.**			***	*
PD	***	***	n.s.	***	***	***	***	**	***	n.s.		
	PC_{cog}	**PC_{mot}**	**PC_{cog}**	**PC_{mot}**	**PC_{cog}**	**PC_{mot}**	**PC_{cog}**	**PC_{mot}**	**PC_{cog}**	**PC_{mot}**	**PC_{cog}**	**PC_{mot}**
	AD		**MCI**		**CON**		**DLB**		**PDD**		**PD**	

Post-hoc-Tests (based on Wilcoxon tests) calculated separately on the two clinical scores MMSE and UPDRS III (top-right/light grey) and the two features PC_{cog} and PC_{mot} (bottom-left/white) between all groups. The comparison between PDD and DLB (bold) is the only combination, which showed insufficient group differences in both topological feature dimensions. The range of the p-value is indicated by the number of stars: * <0.05, ** <0.01, *** <0.001 or n.s. for no significant difference; "-" clinical score not available.